AIMS Materials Science, 9(1): 56–70.
DOI: 10.3934/matersci.2022004
Received: 09 September 2021
Revised: 28 October 2021
Accepted: 02 November 2021
Published: 28 December 2021

http://www.aimspress.com/journal/Materials

Research article

On the determination of first-mode stress intensity factors and T-stress in a continuous functionally graded beam using digital image correlation method

Ahmed M. Abood, Haider Khazal* and Abdulkareem F. Hassan

Department of mechanical engineering, College of engineering, University of Basrah, Basrah, Iraq

* **Correspondence:** Email: haider.mehbes@uobasrah.edu.iq; Tel: +9647816859402.

Abstract: In this study, fracture parameters of epoxy/glass functionally graded composite were determined experimentally using the digital image correlation (DIC) method. A functionally graded material (FGM) with continuous variation in elastic properties was manufactured by gravity casting in vertical template. A 30% volume fraction of glass spheres was dispersed in a low viscosity resin. A single edge crack specimen was examined in a three-point bending test under mode I loading with cracks along the gradient tendency of the material properties. The mechanical properties of FGM were calculated according to ASTM D638. The DIC technique was adopted to obtain the deformation region around the crack tip. William's series was employed to calculate stress intensity factor and T-stress. The experimental results then verified by solving the FE model using ABAQUS program. The comparison between DIC and numerical results illustrated a largely acceptable achievement.

Keywords: continuous FGM; Digital Image Correlation (DIC); three-point bending beam; T-stress; Stress Intensity Factors (SIFs)

1. Introduction

Functionally graded materials (FGMs) are a developed type of composite material designed to obtain new specifications. These specifications differ from those of their individual components and exhibit better performance than traditional composites. The difference in the behavior of FGMs compared to homogenous and other composites is due to the change in their microstructural, chemical and material gradients [1].

Generally, there are two types of gradients in properties that result from their manufacturing method; continuous gradient and stepwise gradient [2,3]. There are various studies in fracture mechanics of FGMs that experimentally and numerically analyze the effect of gradient on the material response. Jin et al. [4] used the concept of crack bridging in FGMs to study the fracture durability and R-curve. They demonstrated that the value of fracture toughness increased with the crack growth from ceramic-rich to metal-rich side when (Alumina-Nickel) FGM was used Dolbow et al. [5] developed a new method for calculating the mixed-mode stress intensity factor SIF using the interaction energy integral method. They employed auxiliary stress and displacement fields as asymptotic domains of areas of discontinuity in a homogenous counterpart that had the same elastic properties as those at the FGM crack tip. SIFs were obtained from the domain integrals which were used as a post-processing in finite element (FE) solution. Butcher et al. [6] prepared an FGM with an elastic modulus that varied spatially. In addition, they used optical interferometry to investigate the crack tip parameters. Rousseau et al. [7–9] and Jain et al. [10] studied the fractures in epoxy-glass FGMs with cracks oriented parallel and perpendicular to the direction of elastic gradient. Optical interferometry was utilized to measure the crack tip deformation in FGM and its homogenous counterpart, which had the same elastic readings in the crack tip. Consequently, two cases were studied: the first one with cracks on the compliant side and the second one on the stiff side. Nakamura et al. [11] submitted a novel method of certain measurement method to estimate the elastic modulus based on the inverse analysis. To simplify the difficulties related to FGM testing, the invers analyses were performed in conjunction with instrumented micro-indentation, employing Kalman filtering (linear quadratic estimation) to investigate the FGM properties.

As well Kim et al. [12] developed a finite element (FE) solution for a stationary crack in an FGM with a smooth gradient in elastic properties. They calculated SIF for mode one, mixed-mode and compared the results which obtained through three different techniques; J-integral, crack-closure, and displacement correlation. Kirugulige et al. [13] studied a cracked FGM under dynamic loading condition applying coherent gradient sensing technique that maps the deformation of the crack tip. A homogenous counterpart was used to elucidate the gradient effect. Khazal et al. [14] determined the fracture parameters of stepwise FGMs (0–60%) volume fraction of glass to produce a five-layer compact tension specimen.

The digital image correlation (DIC) technique was applied to compute the displacement field at the crack tip. Yao et al. [15] adopted DIC method to compute the first mode SIF in epoxy/glass polymer composites. The crack was oriented along the gradient in elastic properties. SIFs and deformity in crack tip zone were calculated in an FGM on both the stiffer and the compliant sides. Jin et al. [16] utilized the DIC technique to study the fracture parameters in an FGM specimen made of ZrO_2/NiCr. They studied the effect of variations in the mechanical properties of ceramic/metal composites which

exposed to a quasi-static mixed-mode. Yates et al. [17] studied the fatigue fracture problem (Mode I in Aluminum alloy) by applied DIC technique to determine the displacement field. SIFS, T-stress and crack tip opening angle were computed by employed William's series. Jones et al. [18] determined mixed mode stress intensity factors in epoxies using digital image correlation. Khazal et al. [19] analyzed the fracture in functionally graded materials where an extended element free Galerkin approach has been used. Additionally, they employed the orthotropic enrichments function to improve the Gauss quadratic accuracy at the crack tip along with the sub-triangle method. Also, the stress intensity factor was computed using incompatible interaction integral technique. The efficiency of XEFGM has been verified when compared the results with the results from references. Khazal and Saleh [20] Presented the crack propagation analysis of FGMs under mixed-mode and non-proportional loading adopting extended element free Galerkin method. SIFs were calculated using the incompatible action integral approach.

The criterion of maximum hoop stress was used to estimate the crack propagation. Good agreement was observed between the simulation results and the references results that were reported in the literature. Mousa et al. [21] presented a study of fracture behaviors in polyester/glass FGM. This polymer matrix composite manufactured by hand lay-up technique and subjected to mixed-mode condition. Experimental and numerical results showed there was an increase in failure load and mode mixity with increasing the crack orientation. Fatima and Rowlands [22] evaluated the SIF in a double edge cracked finite $[0_{13}/90_5/0_{13}]$ graphite-epoxy orthotropic tensile composite using DIC and J integral. They concluded that the presented technique reliable method to estimate SIFs in orthotropic and isotropic materials in comparison with the previous literature. Quanjin et al. [23] employed the DIC technique to investigate the tensile properties in three types of materials which were resin plastic, plastic reinforced with fiber-glass and aluminum A 1100.

As well as, Strain gauge measurement and experimental method. The results show that the DIC had higher values than the experimental method. Abshirini et al. [24] studied the fracture of brittle materials (Polymethylmethacrylate PMMA) to examine the capability of the DIC in evaluating the crack tip parameters in the related materials. Golewski [25,26] studied the effect of adding fly ash to concrete to fracture toughness under mode II using compact tension specimen, on the basis of DIC method a new measurement method for crack tip tracking and accurate determination of crack path length were introduced. The crack tip tracking method has been created can be utilized to analyze and estimate the actual length of crack propagation in various materials. Golewski et al. [27] investigated the effect of curing time to concrete with tow additives fly ash and silica fume under mode I, they found that the mechanical properties of concrete enhanced by this additive.

The present study demonstrates the manufacturing of a continuous functionally graded beam (epoxy/glass FGM) and an experimental investigation of the fracture parameters (T-stress, and stress intensity factors SIFs). The DIC method was adopted to determine the deformation field at the crack tip in a specimen prepared as a three-point bending beam. First-mode SIF and T-stress were evaluated by processing the deformation data in William's equation applying the least square algorithm. The problem was then numerically verified to confirm the accuracy of the DIC technique results.

2. Materials and methods

2.1. Preparation of FGM

The hand lay-up method was utilized to produce a continuous functionally graded beam made of epoxy resin matrix reinforced by glass particles. In this method, an acrylic mold with a length, width and thickness of 300 × 90 × 10 mm is placed vertically. A 30% volume fraction of glass spheres with a mean diameter 90 μm was used to create a composite. Epoxy resin (ρ = 1050 kg/m^3) consists of a two parts base and hardener with a mixing ratio of 1:2. First, the base was mixed with the hardener in a plastic container and stirred well. At the same time, a mixture of glass powder and epoxy was set. Epoxy resin was arranged by mixing the base and hardener in the required proportion. Subsequently, the glass powder was slowly added in small quantities and was continuously stirred until the whole amount of glass powder was mixed with the epoxy resin. The first step in the pouring process was pouring the pure epoxy resin until it reached half of the mould and then leaving it for certain time. Thereafter, the epoxy-glass mixture was added to the mould, which was sufficient to completely fill it. Then, the mould was sealed, flipped upside down and kept it in a vertical position; and flipped again before being left to cure at room temperature. Subsequently, the mould was dissociated and the FGM beam was extracted. The percentage of glass volume fraction in this FGM was calculated using Image-J software to analyses the microscopic images. A portion of the produced beam was cut in the direction of the gradient, then divided into 1.5 × 1 cm piece and examined under microscope (Figure 1).

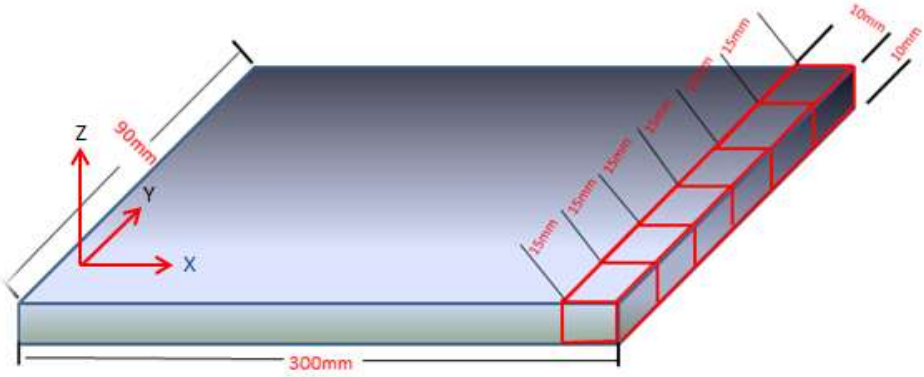

Figure 1. FGM specimen with spatial gradient.

2.2. Determination of mechanical properties

Standard FGM tensile test samples were machined from the functionally graded beam according to ASTM D638 to extract the elastic properties. Standard dog bone type I was selected where the thickness of the specimen is 7 mm; the overall length is 165 mm, the gauge length is 57 mm, the width of the narrow side is 13 mm, and the fillet radius is 76 mm as shown in Figure 2. The examination process was done by using INSTRON device with test speed 5 mm per min as cleared in Figure 3. Table 1 illustrates the elastic properties of the corresponding volume fractions of glass.

Figure 2. Standard tensile test specimens.

Figure 3. Tensile test process.

Table 1. Elasticity Modulus and Poisson's ratio corresponding to the volume fraction.

Young's modulus (MPa)	Poisson's ratio	Volume fraction
1128	0.39	0.0
1130	0.34	0.027
1885	0.32	0.213
2230	0.31	0.261
2618	0.3	0.298

The influence of the volume fraction on the Young's modulus of the produced FGM is shown in Table 1. Furthermore, increasing the volume fraction contributes to an increase in stiffness of relevant sample. As the volume fraction increases, the Poisson's ratio of the manufactured FGM.

2.3. DIC

2.3.1. Preparing the specimen

The basic principle of the DIC technique is depends on the comparison of two digital images: one before loading, known as reference; and the other one after deformation known as the deformed. This process was accomplished artificially by applying a white background on the specimen surface and black speckles to create a random pattern the size of the speckles is 3 to 25 pixels and the distance between them is 3 to 20 pixels, as shown in Figure 4. The intensity of light can be specified for each pixel by discretizing the intensity of the specific area into a number range known as grey scale, and then tracing the same small area of the specimen in the reference and deformed images by using a suitable computer program. This small area consists of different pixels and different grey scale is called subset. In this technique, a comparison was performed between each subset in the reference and deformed images to compute the correlation coefficient. The subset size and subset spacing play important roles in determining SIFs [28].

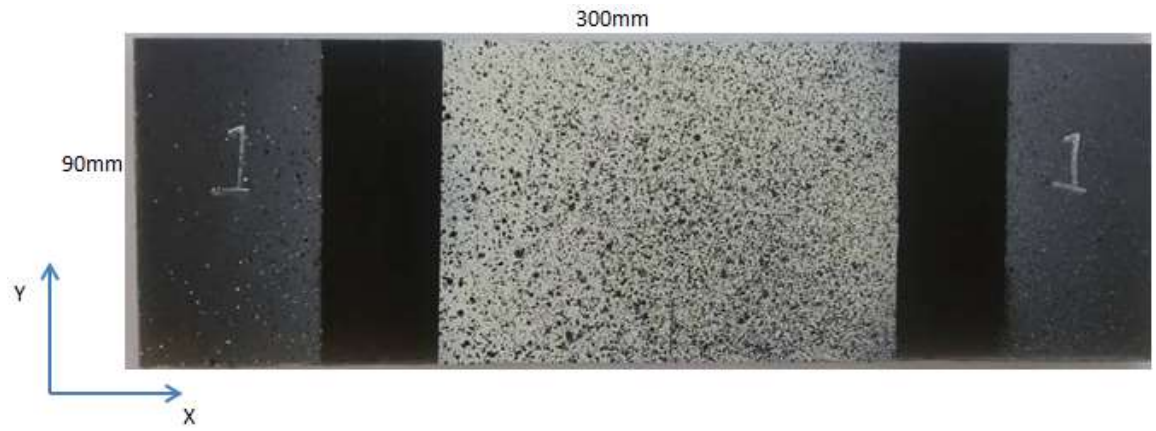

Figure 4. Preparation of the specimen by making a speckles pattern.

The FGM specimen was tested as a three-point bending beam by applying a first mode loading condition (Figure 5). A 19.3 mm long single-edge crack was created in the FGM sample on the compliant (epoxy-rich) side along the gradient direction. The distance between specimen and the lens was 50 cm and the camera was set perpendicular to the specimen, the lens parameters and light location were changed to reach the best contrast and uniform light. All moving components in the mounting system had been locked after determine the final position and orientation. A GOTCH machine was used in the test at grip speed 1 mm/min. An ARTCAM-320p CCD camera with resolution (2288 × 1700) pixels was employed for imaging, as depicted in Figure 6.

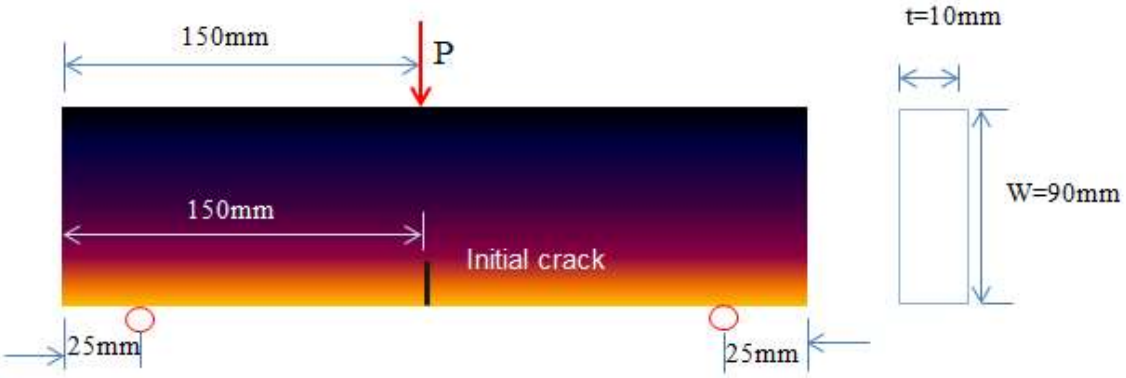

Figure 5. Crack in a beam subjected to three-point bending.

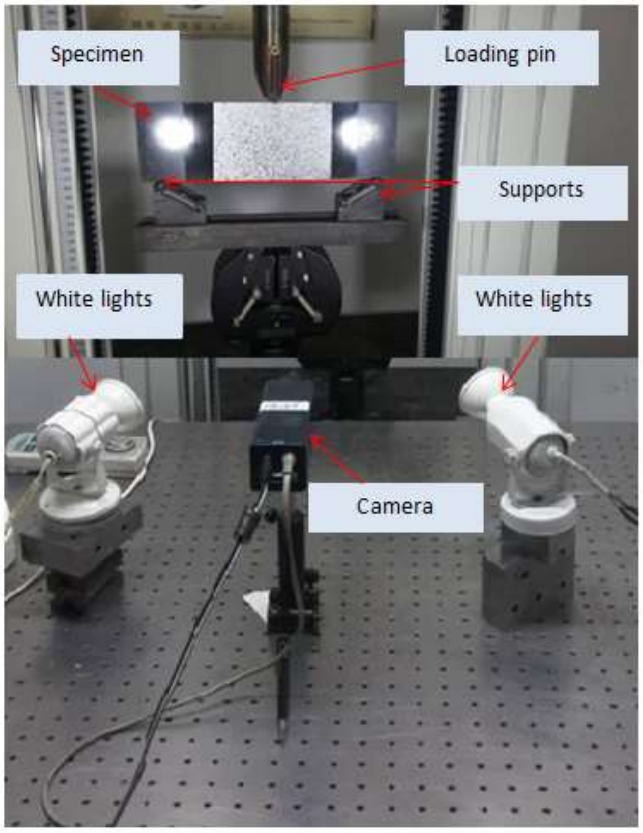

Figure 6. Normal mode tests.

2.3.2. Evaluation of SIF and T-stress

William's methodology was involved to evaluate T-stress and SIF values from the deformation field in the crack-tip region. The crack-tip location had to be identified in advance, because the SIFs values depend on the crack-tip coordinates that set in the algorithm. The infinite series that represents the displacement field can be written as [17]:

$$\text{Mode I} \begin{Bmatrix} u_1 = \sum_{n=1}^{\infty} \frac{r^{\frac{n}{2}}}{2\mu} c_n \left\{ \left[\kappa + \frac{n}{2} + (-1)^n \right] cos\frac{n\theta}{2} - \frac{n}{2} cos\frac{(n-4)\theta}{2} \right\} \\ v_1 = \sum_{n=1}^{\infty} \frac{r^{\frac{n}{2}}}{2\mu} c_n \left\{ \left[\kappa - \frac{n}{2} - (-1)^n \right] sin\frac{n\theta}{2} + \frac{n}{2} sin\frac{(n-4)\theta}{2} \right\} \end{Bmatrix} \quad (1)$$

and,

$$\text{Mode II} \begin{Bmatrix} u_{II} = -\sum_{n=1}^{\infty} d_n \left\{ \left[\kappa + \frac{n}{2} - (-1)^n \right] sin\frac{n\theta}{2} - \frac{n}{2} sin\frac{(n-4)\theta}{2} \right\} \\ v_{II} = \sum_{n=1}^{\infty} d_n \left\{ \left[\kappa - \frac{n}{2} + (-1)^n \right] cos\frac{n\theta}{2} + \frac{n}{2} cos\frac{(n-4)\theta}{2} \right\} \end{Bmatrix} \quad (2)$$

Where, u, v are the components of the horizontal and vertical displacement, respectively, μ is the rigidity modulus. For plane stress κ = (3 − ν)/ (1 + ν) and for plane strain κ = (3 − 4ν). c and d are constants that had to be calculated, while c_1, d_1 refer to mode I and mode II SIFs, T-stress also can be evaluated when n = 2, (r, ɵ) are the crack-tip polar coordinate. In Eqs 1 and 2, the displacement field can be defined as:

$$p_{n,m} = \frac{r_m^{\frac{n}{2}}}{2\mu} \left\{ \left[\kappa + \frac{n}{2} + (-1)^n \right] cos\frac{n\theta_m}{2} - \frac{n}{2} cos\frac{(n-4)\theta_m}{2} \right\} \quad (3)$$

$$q_{n,m} = \frac{-r_m^{\frac{n}{2}}}{2\mu} \left\{ \left[\kappa + \frac{n}{2} - (-1)^n \right] sin\frac{n\theta_m}{2} - \frac{n}{2} sin\frac{(n-4)\theta_m}{2} \right\} \quad (4)$$

$$w_{n,m} = \frac{r_m^{\frac{n}{2}}}{2\mu} \left\{ \left[\kappa - \frac{n}{2} - (-1)^n \right] sin\frac{n\theta_m}{2} + \frac{n}{2} sin\frac{(n-4)\theta_m}{2} \right\} \quad (5)$$

$$z_{n,m} = \frac{r_m^{\frac{n}{2}}}{2\mu} \left\{ \left[\kappa - \frac{n}{2} + (-1)^n \right] cos\frac{n\theta_m}{2} + \frac{n}{2} cos\frac{(n-4)\theta_m}{2} \right\} \quad (6)$$

$$\begin{Bmatrix} u_1 \\ . \\ . \\ . \\ u_m \\ v_1 \\ . \\ . \\ . \\ v_m \end{Bmatrix} = \begin{bmatrix} p_{1,1} \ldots p_{n,1} & q_{1,1} \ldots q_{n,1} \\ & . \\ & . \\ & . \\ p_{1,m} \ldots p_{n,m} & q_{1,m} \ldots q_{n,m} \\ w_{1,1} \ldots w_{n,1} & z_{1,1} \ldots z_{n,1} \\ & . \\ & . \\ & . \\ w_{1,m} \ldots w_{n,m} & z_{1,m} \ldots z_{n,m} \end{bmatrix} \begin{Bmatrix} c_1 \\ . \\ . \\ . \\ c_n \\ d_1 \\ . \\ . \\ . \\ d_n \end{Bmatrix} \quad (7)$$

Where m is the index of the data point; $p_{n,m}$, $q_{n,m}$, $w_{n,m}$, and $z_{n,m}$ are the known functions of (r, ɵ). Furthermore, expanding Eqs 1 and 2 using the T-stress and SIF as shown in the following equations

$$u = \frac{KI}{2\mu}\sqrt{\frac{r}{2\pi}} cos\frac{\theta}{2}\left(\kappa - 1 + 2\,sin^2\frac{\theta}{2}\right) + \frac{KII}{2\mu}\sqrt{\frac{r}{2\pi}} sin\frac{\theta}{2}\left(\kappa + 1 + 2\,cos^2\frac{\theta}{2}\right) + \frac{T}{8\mu} r(\kappa + 1) cos\theta \quad (8)$$

$$v= \frac{KI}{2\mu}\sqrt{\frac{r}{2\pi}}sin\frac{\theta}{2}\left(\kappa+1-2\,cos^2\frac{\theta}{2}\right)-\frac{KII}{2\mu}\sqrt{\frac{r}{2\pi}}cos\frac{\theta}{2}\left(\kappa-1-2\,cos^2\frac{\theta}{2}\right)+\frac{T}{8\mu}r(\kappa-3)sin\theta \tag{9}$$

It can be exhibited that:

$$K_I= c_1\sqrt{2\pi},\ K_{II}= -d_1\sqrt{2\pi},\ T = 4c_2 \tag{10}$$

Where K_I is SIF for mode I, K_{II} is the SIF for mode II, and T is the T-stress.
By adding constants to Eq 7, rigid body motion and translation can be compensated.

$$\begin{Bmatrix} u_1 \\ \cdot \\ \cdot \\ \cdot \\ u_m \\ v_m \\ \cdot \\ \cdot \\ \cdot \\ v_m \end{Bmatrix} = \begin{bmatrix} 1 & p_{1,1}\ \ldots\ p_{n,1} & 0 & q_{1,1}\ \ldots\ q_{n,1} & -rsin\theta_1 \\ & \cdot & & \cdot & \\ & \cdot & & \cdot & \\ & \cdot & & \cdot & \\ 1 & p_{1,m}\ \ldots\ p_{n,m} & 0 & q_{1,m}\ \ldots\ q_{n,m} & -rsin\theta_m \\ 0 & w_{1,1}\ \ldots\ w_{n,1} & 1 & z_{1,1}\ \ldots\ z_{n,1} & r_1 sin\theta_1 \\ & \cdot & & \cdot & \\ & \cdot & & \cdot & \\ & \cdot & & \cdot & \\ 0 & w_{1,m}\ \ldots\ w_{n,m} & 1 & z_{1,m}\ \ldots\ z_{n,m} & r_m cos\theta_m \end{bmatrix} \begin{Bmatrix} c_0 \\ c_1 \\ \cdot \\ \cdot \\ \cdot \\ c_n \\ d_0 \\ d_1 \\ \cdot \\ \cdot \\ \cdot \\ d_n \\ R \end{Bmatrix} \tag{11}$$

Where c_0, d_0 are used to compensate the rigid body translation and R is used to compensate the rigid body rotation.

3. Results and discussion

3.1. Mechanical properties

Referring to Table 1 plotting volume fraction of glass content with corresponding elastic modulus pointed a direct relationship between them. Figures 7 and 8 Clarify, respectively, that Young's modulus increased while Poisson's ratio decreased as the volume fraction of filler particles increased.

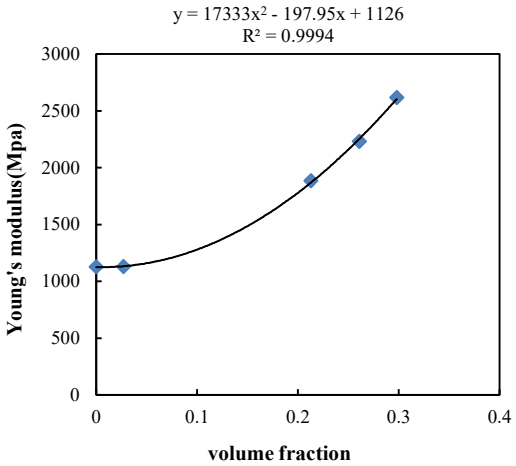

Figure 7. Relationships between volume fraction of glass particles and elastic modulus.

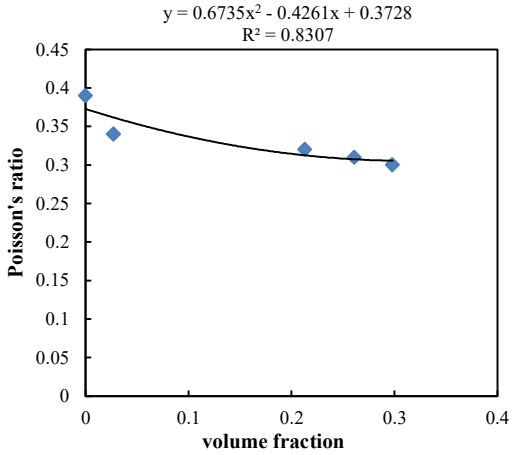

Figure 8. Relationship between volume fraction of glass particles and Poisson's ratio.

3.2. DIC results

After calculating the displacement field from DIC test the post processing step must be done to estimate the fracture parameters by considering the area of collected data. These steps were accomplished by applying the displacement infinite series (William's series). The numerical solution of the first mode loading of the FG beam with a 19.3 mm edge crack was performed by ABAQUS program using contour integral approach. C3D8R element type is selected. Mesh configuration, B.C and loading as shown in Figure 9. The X and Y displacement fields of the three-point bend specimen at 2246.5 N for experimental and numerical results are illustrated in Figure 10.

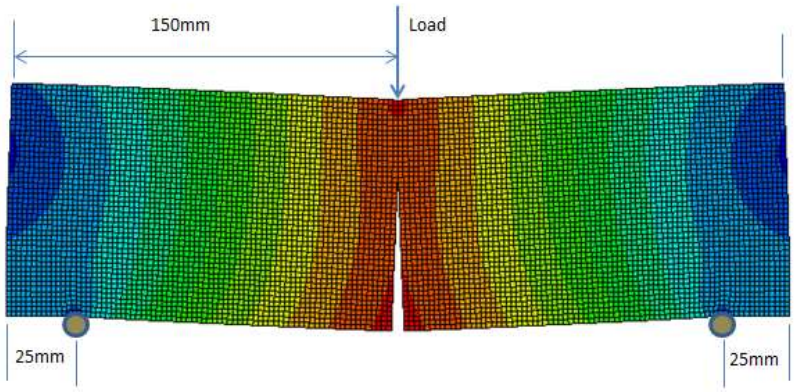

Figure 9. Mesh configuration.

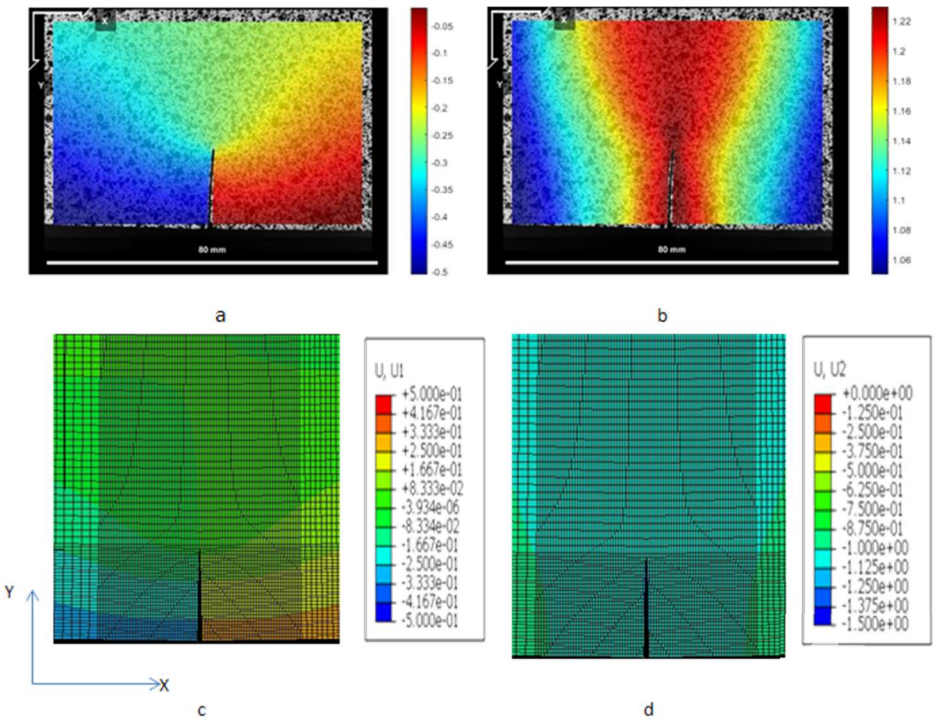

Figure 10. Displacement field in X and Y directions at 2245 N obtained with (a), (b) DIC, and (c), (d) FE.

The main challenge is to build an appropriate proportion of terms in William's equations and the data collection area. During the verification process, the number of terms in William's series increase until the values of T-stresses and SIFs converge, as depicted in Figure 11. The calculated values of DIC measurements for different numbers of terms are listed in Table 2.

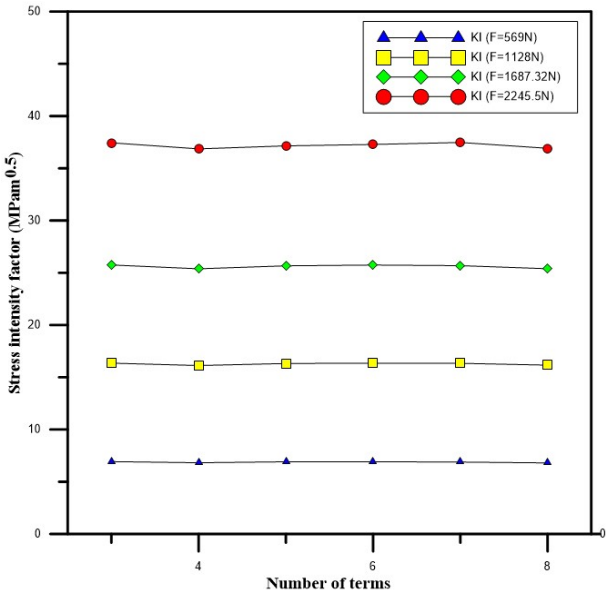

Figure 11. Convergence of SIF in terms of the number of terms in William's equation.

Table 2. Experimental data of SIF (KI) and T-stress at different loads and number of terms.

Load (N)	Number of terms	KI ($MPam^{0.5}$)	T-stress (MPa)	Load (N)	Number of terms	KI ($MPam^{0.5}$)	T-stress (MPa)
569	3	6.927	0.527	1687.32	3	25.75	1.438
	4	6.813	0.510		4	25.382	1.391
	5	6.906	0.448		5	25.666	1.159
	6	6.916	0.430		6	25.741	1.090
	7	6.882	0.325		7	25.686	0.788
1128	3	16.353	1.019	2246.5	3	37.44	1.929
	4	16.128	0.998		4	36.862	1.824
	5	16.316	0.841		5	37.152	1.661
	6	16.347	0.799		6	37.285	1.547
	7	16.336	0.617		7	37.471	1.142

Figure 11 clarifies that good verification and stability in SIFs values in terms of the number of terms in William's equation. Tables 3 and 4 illustrate the exprimental and numerical results with relative error between them.

Table 3. Relative error between DIC and FE of SIFs results at loads 569–2246.5 N for normal mode loading.

Load (N)	KI (DIC)	KI (FE)	Relative error %
569	6.927	6.941	0.202
1128	16.128	16.193	0.403
1687.32	25.382	24.841	2.1
2246.5	36.862	37.486	1.69

Table 4. Relative error between DIC and FE of T-stress results at loads 569–2246.5 N for normal mode loading.

Load (N)	T (DIC)	T (FE)	Relative error %
569	0.51	0.583	14
1128	0.967	0.998	3.1
1687.32	1.43	1.391	2.8
2246.5	1.925	1.824	5.5

The experimental and numerical results for SIF and T-stress of the epoxy/glass FGM exhibited good agreement.

4. Conclusion

The results of this work indicate that the important conclusions can be illustrated as follow:

(1) The process that adopted in manufacturing continuous FGM was efficient method to produce monotonic variation in elastic moduli. All manufacturing processes were implemented at room temperature.
(2) The manufacturing of this important FG beam which has a functional gradation in the properties of the material can be used in the analysis of more fracture problems or vibration problems.
(3) The DIC results based on experimental technique compared with numerical results demonstrated that the DIC approach is successful method of evaluating fracture parameters. The average relative error for SIF (KI) and T-stress are 1.095%, 6.35% respectively for first mode.
(4) The DIC results show good stabilization and verification in SIFs during the variation of the number of terms in William's series at different loads.
(5) Good agreement has been observed between DIC and FE results for SIFs (KI) for first mode.
(6) The T-stress values based on experimental and numerical results shows 14% relative error at load 569 N because of the T-stress was computed from high order terms of displacement field as stated in [14] and [17].

Acknowledgements

The authors thank the IBEM lab in the University of Tehran for helping to conduct DIC test.

Conflict of interest

The authors confirm that this article content has no conflict of interest.

References

1. Pei G, Asaro RJ (1997) Cracks in functionally graded materials. *Int J Solids Struct* 34: 1–17. https://doi.org/10.1016/0020-7683(95)00289-8
2. Miyamoto Y, Kaysser WA, Rabin BH, et al. (2013) *Functionally Graded Materials: Design, Processing and Applications*, New York: Springer Science & Business Media.
3. Farouq W, Khazal H, Hassan AKF (2019) Fracture analysis of functionally graded material using digital image correlation technique and extended element-free Galerkin method. *Opt Laser Eng* 121: 307–322. https://doi.org/10.1016/j.optlaseng.2019.04.021
4. Jin ZH, Batra RC (1996) Some basic fracture mechanics concepts in functionally graded materials. *J Mech Phys Solids* 44: 1221–1235. https://doi.org/10.1016/0022-5096(96)00041-5
5. Dolbow JE, Gosz M (2002) On the computation of mixed-mode stress intensity factors in functionally graded materials. *Int J Solids Struct* 39: 2557–2574. https://doi.org/10.1016/S0020-7683(02)00114-2

6. Butcher RJ, Rousseau CE, Tippur HV (1998) A functionally graded particulate composite: prepa ration, measurements and failure analysis. *Acta Mater* 47: 259–268. https://doi.org/10.1016/S13 59-6454(98)00305-X
7. Rousseau CE, Tippur HV (2002) Evaluation of crack tip fields and stress intensity factors in functionally graded elastic materials: cracks parallel to elastic gradient. *Int J Fracture* 114: 87–112. https://doi.org/10.1023/A:1014889628080
8. Rousseau CE, Tippur HV (2000) Compositionally graded materials with cracks normal to the elastic gradient. *Acta Mater* 48: 4021–4033. https://doi.org/10.1016/S1359-6454(00)00202-0
9. Rousseau CE, Tippur HV (2002) Influence of elastic variations on crack initiation in functionally graded glass-filled epoxy. *Eng Fract Mech* 69: 1679–1693. https://doi.org/10.1016/S0013-7944(02)00056-5
10. Jain N, Rousseau CE, Shukla A (2004) Crack-tip stress fields in functionally graded materials with linearly varying properties. *Theor Appl Fract Mec* 42: 155–170. https://doi.org/10.1016/j.tafmec.2004.08.005
11. Nakamura T, Wang T, Sampath S (2000) Determination of properties of graded materials by inverse analysis and instrumented indentation. *Acta Mater* 48: 4293–4306. https://doi.org/10.1016/S1359-6454(00)00217-2
12. Kim JH, Paulino GH (2002) Finite element evaluation of mixed mode stress intensity factors in functionally graded materials. *Int J Numer Methods Eng* 53: 1903–1935. https://doi.org/10.1002/nme.364
13. Kirugulige MS, Tippur HV (2006) Mixed-mode dynamic crack growth in functionally graded glass-filled epoxy. *Exp Mech* 46: 269–281. https://doi.org/10.1007/s11340-006-5863-4
14. Khazal H, Hassan AKF, Farouq W, et al. (2019) Computation of fracture parameters in stepwise functionally graded materials using digital image correlation technique. *Mater Perform Charac* 8: 344–354. https://doi.org/10.1520/MPC20180175
15. Yao XF, Xiong TC, Xu W, et al. (2006) Experimental investigations on deformation and fracture behavior of glass sphere filled epoxy functionally graded materials. *Appl Compos Mater* 13: 407–420. https://doi.org/10.1007/s10443-006-9026-7
16. Jin X, Wu L, Guo L, et al. (2009) Experimental investigation of the mixed-mode crack propagati on in ZrO_2/NiCr functionally graded materials. *Eng Fract Mech* 76: 1800–1810. https://doi.org/1 0.1016/j.engfracmech.2009.04.003
17. Yates JR, Zanganeh M, Tai YH (2010) Quantifying crack tip displacement fields with DIC. *Eng Fract Mech* 77: 2063–2076. https://doi.org/10.1016/j.engfracmech.2010.03.025
18. Jones SA, Tomlinson RA (2015) Investigating mixed-mode (I/II) fracture in epoxies using digital image correlation: Composite GIIc performance from resin measurements. *Eng Fract Mech* 149: 368–374. https://doi.org/10.1016/j.engfracmech.2015.08.041
19. Khazal H, Bayesteh H, Mohammadi S, et al. (2016) An extended element free Galerkin method for fracture analysis of functionally graded materials. *Mech Adv Mater Struc* 23: 513–528. https: //doi.org/10.1080/15376494.2014.984093
20. Khazal H, Saleh NA (2019) XEFGM for crack propagation analysis of functionally graded materials under mixed-mode and non-proportional loading. *Mech Adv Mater Struc* 26: 975–983. https://doi.org/10.1080/15376494.2018.1432786

21. Mousa S, Abd-Elhady AA, Abu-Sinna A, et al. (2019) Mixed mode crack growth in functionally graded material under three-point bending. *Pro Struc Int* 17: 284–291. https://doi.org/10.1016/j.prostr.2019.08.038
22. Fatima NS, Rowlands RE (2020) SIF determination in finite double-edge cracked orthotropic composite using J-integral and digital image correlation. *Eng Fract Mech* 235: 107099. https://doi.org/10.1016/j.engfracmech.2020.107099
23. Quanjin M, Rejab MRM, Halim Q, et al. (2020) Experimental investigation of the tensile test usi ng digital image correlation (DIC) method. *Mater Today* 27: 757–763. https://doi.org/10.1016/j. matpr.2019.12.072
24. Abshirini M, Dehnavi MY, Beni MA, et al. (2014) Interaction of two parallel U-notches with tip cracks in PMMA plates under tension using digital image correlation. *Theor Appl Fract Mec* 70: 75–82. https://doi.org/10.1016/j.tafmec.2014.02.001
25. Golewski GL (2021) Evaluation of fracture processes under shear with the use of DIC technique in fly ash concrete and accurate measurement of crack path lengths with the use of a new crack tip tracking method. *Measurement* 181: 109632. https://doi.org/10.1016/j.measurement.2021.109632
26. Golewski GL (2021) Validation of the favorable quantity of fly ash in concrete and analysis of crack propagation and its length–Using the crack tip tracking (CTT) method–In the fracture toughness examinations under Mode II, through digital image correlation. *Constr Build Mater* 296: 122362. https://doi.org/10.1016/j.conbuildmat.2021.122362
27. Golewski GL, Gil DM (2021) Studies of fracture toughness in concretes containing fly ash and silica fume in the first 28 days of curing. *Mater* 14: 319. https://doi.org/10.3390/ma14020319
28. Eshraghi I, Dehnavi MRY, Soltani N (2014) Effect of subset parameters selection on the estimation of mode-I stress intensity factor in a cracked PMMA specimen using digital image correlation. *Polym Test* 37: 193–200. https://doi.org/10.1016/j.polymertesting.2014.05.017

AIMS Press